


Topological crystalline insulators with C_2 rotation anomalyTan Zhang ^{1,2} Changming Yue,^{1,2} Tiantian Zhang,^{1,2} Simin Nie,^{3,*} Zhijun Wang,^{1,4}
Chen Fang,^{1,2,4,5} Hongming Weng,^{1,2,4,5,†} and Zhong Fang^{1,2}¹Beijing National Research Center for Condensed Matter Physics, and Institute of Physics,
Chinese Academy of Sciences, Beijing 100190, China²School of Physical Sciences, University of Chinese Academy of Sciences, Beijing 100049, China³Department of Materials Science and Engineering, Stanford University, Stanford, California 94305, USA⁴CAS Center for Excellence in Topological Quantum Computation, University of Chinese Academy of Sciences, Beijing 100190, China⁵Songshan Lake Materials Laboratory, Dongguan, Guangdong 523808, China

(Received 21 May 2019; published 9 August 2019)

Based on first-principles calculations and a symmetry-based indicator analysis, we find a class of topological crystalline insulators (TCIs) with a C_2 rotation anomaly in a family of Zintl compounds, including $Ba_3Cd_2As_4$, $Ba_3Zn_2As_4$, and $Ba_3Cd_2Sb_4$. The nontrivial band topology protected by the coexistence of C_2 rotation symmetry and time-reversal symmetry T leads to two surface Dirac cones at generic momenta on both top and bottom surfaces perpendicular to the rotation axis. In addition, $(d - 2)$ -dimensional helical hinge states are also protected along the hinge formed by two side surfaces parallel to the rotation axis. We develop a method based on the nested Wilson loop technique to prove the existence of these surface Dirac cones due to a C_2 anomaly and precisely locate them as demonstrated in studying these TCIs. The helical hinge states are also calculated. Finally, we show that external strain can be used to tune the topological phase transitions among TCIs, strong Z_2 topological insulators, and trivial insulators.

DOI: [10.1103/PhysRevResearch.1.012001](https://doi.org/10.1103/PhysRevResearch.1.012001)

Introduction. The fermion multiplication theorem is a generalization of the fermion doubling theorem in particle physics to crystalline solids. For example, in a two-dimensional (2D) system with a time-reversal symmetry of $T^2 = -1$ and n -fold rotational symmetry C_n ($n = 2, 4, 6$), this theorem imposes a restriction on the number of stable massless Dirac fermions due to a linear band crossing at arbitrarily generic momenta. The number of Dirac nodes must be a multiple of $2n$ in the first Brillouin zone (BZ) and they are robust against arbitrary perturbations preserving T and C_n . Recently, quantum anomalies associated with discrete rotational symmetry $C_{n=2,4,6}$ and time-reversal symmetry T have been proposed, which limit the number of massless fermions at generic momenta to be a multiple of n instead of $2n$ in two dimensions [1]. Such a rotation anomaly can only happen on the top or bottom surface of a three-dimensional (3D) system when the surfaces are perpendicular to the rotation axis [1]. As we know, a single massless Dirac fermion with a parity anomaly appears on the surface of a 3D topological insulator (TI) with time-reversal symmetry [2–6]. The rotation anomaly leads to a new class of 3D TCIs [7–10]. Their surface states consist of n Dirac cones, which evades the above fermion multiplication

theorem. Furthermore, they support n one-dimensional (1D) helical modes on the hinge formed by two side surfaces parallel to the rotation axis [11–15].

There have been several materials proposed to have the above rotational anomaly. One of them is SnTe [16], a well-known TCI protected by mirror symmetry with a nonzero mirror Chern number. On its (110) surface, the two surface Dirac cones, which have been thought to be protected by mirror symmetry, cannot be gapped if the mirror symmetry is broken while C_2 and T are still preserved. Similarly, the four Dirac cones on the (001) surface can also be understood to be protected by C_4 and T symmetries [17]. The other example is antiperovskite Sr_3PbO [18]. On its (001) surface, there are four Dirac cones due to the C_4 anomaly. The Ca_2As family is found to be TCIs protected by rotation symmetry, which have two Dirac cones at generic locations in momentum space if the mirror symmetry is broken, but the rotational and time-reversal symmetries are preserved [19]. Recently, one phase of BiBr compounds has also been proposed to be a TCI with a C_2 rotation anomaly [20,21], and the surface Dirac cones and hinge states are also calculated.

As a new class of TCIs, the corresponding topological invariant ν_{C_n} can be defined, although it is very difficult to obtain them. Recently, a convenient method to identify these topologically nontrivial insulators has been proposed and programmed to screen all known nonmagnetic compounds [22,23]: the explicit and exhaustive mappings from symmetry data, band representations at high symmetric momenta, to topological indicators for arbitrary gapped band structures in the presence of time-reversal symmetry and all of the 230 space groups. The symmetry data of any gapped band structure can

*smnie@stanford.edu

†hmweng@iphy.ac.cn

Published by the American Physical Society under the terms of the [Creative Commons Attribution 4.0 International](https://creativecommons.org/licenses/by/4.0/) license. Further distribution of this work must maintain attribution to the author(s) and the published article's title, journal citation, and DOI.

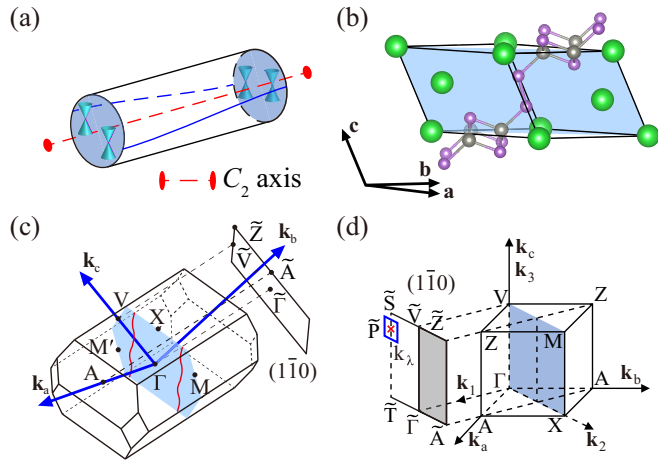


FIG. 1. (a) The topological boundary states due to the C_2 anomaly. For a cylinderlike sample, there are two Dirac cones on both the top and bottom surfaces and two 1D helical hinge states. (b) The primitive cell of $\text{Ba}_3\text{Cd}_2\text{As}_4$. The green, gray, and purple balls represent Ba, Cd, and As atoms, respectively. The blue plane is the mirror plane. **a**, **b**, and **c** are three primitive lattice vectors. (c) The first BZ of bulk and the $(1\bar{1}0)$ surface BZ. The mirror plane is marked as blue and the nodal lines in it are marked red. (d) The schematic diagram of BZ in reciprocal lattices \mathbf{k}_a , \mathbf{k}_b , and \mathbf{k}_c and the redefined ones \mathbf{k}_1 , \mathbf{k}_2 , and \mathbf{k}_3 , with \mathbf{k}_1 along the C_2 rotation axis and \mathbf{k}_2 , \mathbf{k}_3 being lattice vectors for the $(1\bar{1}0)$ surface BZ, where one of the calculated surface Dirac cones is marked as a red cross at \tilde{P} surrounded by a loop in blue lines.

be compressed into a set of up to four $\mathbb{Z}_{m=2,3,4,6,8,12}$ numbers called symmetry-based indicators (SIs). This progress [23–25] has greatly accelerated the discovery of new topological materials.

We find that three Zintl compounds, namely, $\text{Ba}_3\text{Cd}_2\text{As}_4$, $\text{Ba}_3\text{Zn}_2\text{As}_4$, and $\text{Ba}_3\text{Cd}_2\text{Sb}_4$, are TCIs classified by the C_2 anomaly. We show the detailed and systematic method to judge a material with a C_2 anomaly and prove the existence of a surface Dirac cone with the nested Wilson loop technique. They have two surface Dirac cones protected by C_2 and time-reversal symmetry T at arbitrary momenta on both the top and bottom $(1\bar{1}0)$ surfaces, as shown in Fig. 1. Besides, the two Dirac cones are connected by two helical hinge states on the side surface. Compared with SnTe , Sr_3PbO , and the Ca_2As family, the proposed Zintl compounds have no mirror planes passing through the C_2 rotation axis and the surface Dirac cones will be at a generic momentum instead of being constrained by the mirror planes. This makes the C_2 rotation anomaly clearer. Comparing with BiBr , the difference is that the symmetry indicator is (0002) for BiBr , but (1102) for the Zintl compounds. The nontrivial Z_2 weak invariants indicate that the Zintl compounds have additional topological surface states.

Crystal structure and methodology. The Zintl compounds $\text{Ba}_3\text{Cd}_2\text{As}_4$, $\text{Ba}_3\text{Zn}_2\text{As}_4$, and $\text{Ba}_3\text{Cd}_2\text{Sb}_4$ have been synthesized by Pb-flux methods and routine solid-state techniques in recent years [26,27], and possess abundant novel physical properties [28–30]. The crystallographic data and the atomic coordinates for these materials are listed in the Supplemental Material [31]. They all crystallize in the same

crystal structure, and $\text{Ba}_3\text{Cd}_2\text{As}_4$ is selected as an example to illustrate the structure, as shown in Fig. 1(b). The structure can be concisely described as stacked Cd_2As_4 layers which are separated by Ba cations. The space group is $C2/m$ (No. 12) which has inversion symmetry P , rotation symmetry $C_2:(a, b, c) \rightarrow (-b, -a, -c)$, and mirror symmetry $M_{1\bar{1}0}:(a, b, c) \rightarrow (b, a, c)$.

For an inversion symmetric system, the SIs $\mathbb{Z}_{2,2,2,4} = (z_{2,1}, z_{2,2}, z_{2,3}, z_4)$ are defined to indicate a new topological classification,

$$z_{2,\varepsilon} \equiv \sum_{\substack{\mathbf{K} \in \text{TRIM} \\ \text{at } \{k_\varepsilon = \pi, \varepsilon = 1, 2, 3\}}} \frac{n_-^{\mathbf{K}} - n_+^{\mathbf{K}}}{2} \bmod 2,$$

$$z_4 \equiv \sum_{\mathbf{K} \in \text{TRIM}} \frac{n_-^{\mathbf{K}} - n_+^{\mathbf{K}}}{2} \bmod 4, \quad (1)$$

where $n_{\pm}^{\mathbf{K}}$ is the number of occupied Kramers pairs having even (odd) parity at time-reversal invariant momenta (TRIM). The three $z_{2,\varepsilon}$ invariants are equal to the three weak Z_2 topological invariants. When z_4 is 1 or 3, it indicates a strong TI, similar to the strong topological Z_2 invariant. When it is zero, the system is a weak TI if any one of $z_{2,\varepsilon}$ is nonzero, while $z_4 = 2$ means a TCI.

The method of calculating the Berry phase of the Wilson loop eigenfunctions is used to prove the existence of surface Dirac cones at generic momenta. For a 3D system, its tight-binding Hamiltonian satisfies

$$H(k_1, k_\lambda)|u_n(k_1, k_\lambda)\rangle = E_n(k_1, k_\lambda)|u_n(k_1, k_\lambda)\rangle, \quad (2)$$

where k_1 is along the periodical path in the bulk BZ perpendicular to the surface of loop k_λ . We define an overlap matrix for n_{occ} occupied states as $M_{mn}(k_\alpha, k_{\alpha+1}) = \langle u_m(k_\alpha, k_\lambda)|u_n(k_{\alpha+1}, k_\lambda)\rangle$ ($m, n = 1, 2, \dots, n_{\text{occ}}$) [12,32]. Thus, the Wilson loop $\mathcal{W}(k_\lambda)$ is defined as

$$\mathcal{W}(k_\lambda) = \prod_{\alpha=0}^{N_1-1} M(k_\alpha, k_{\alpha+1}), \quad (3)$$

where the loop consisting of N_1 discretized k_α points with $k_{\alpha=N_1} = k_{\alpha=0} + G_1$ (G_1 is the length of the reciprocal lattice vector along the k_1 loop). We can diagonalize $\mathcal{W}(k_\lambda)$ and get the eigenvalue $W_i(k_\lambda) = \exp[i\theta_i(k_\lambda)]$ and the corresponding eigenvectors $\tilde{w}_i(k_\lambda)$. $\theta_i(k_\lambda)$ is referred to as a 1D hybrid Wannier center along k_1 , which is also known as the i th Wilson loop flow along the loop k_λ [33].

We define a new overlap matrix for a selected n' number of Wilson eigenvectors as $\tilde{M}_{\tilde{m}\tilde{n}}(k_\lambda, k_{\lambda+1}) = \langle \tilde{w}_{\tilde{m}}(k_\lambda)|\tilde{w}_{\tilde{n}}(k_{\lambda+1})\rangle$ ($\tilde{m}, \tilde{n} = 1, 2, \dots, n'$) [12], and the nested Wilson loops along the closed loop consisting of N' discretized k_λ points with $k_{\lambda=N'} = k_{\lambda=0}$ are

$$\tilde{\mathcal{W}} = \prod_{\lambda=0}^{N'-1} \tilde{M}(k_\lambda, k_{\lambda+1}). \quad (4)$$

Further, the Berry phase [34,35] is written as

$$\phi = -\text{Im} \ln \det \tilde{\mathcal{W}}. \quad (5)$$

If the (n') th Wilson loop flow and the $(n'+1)$ th one cross each other and the crossing point is enclosed by the selected

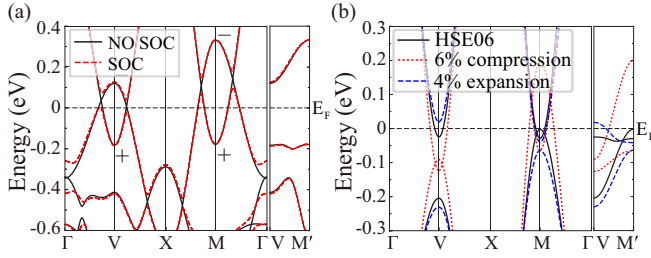


FIG. 2. (a) The band structures of $\text{Ba}_3\text{Cd}_2\text{As}_4$. The black solid and red dashed curves represent the bands from GGA calculations without and with SOC, respectively. The + (−) indicates the parity of two inverted bands at the V and M points. (b) The band structures from HSE06 calculations. The black solid, red dotted, and blue dashed curves represent the bands with no strain, 6% compression, and 4% expansion of the lattice constants, respectively.

loop k_λ , the Berry phase ϕ from Eq. (5) will be π , or it will be zero.

Band structures and bulk topology. We choose $\text{Ba}_3\text{Cd}_2\text{As}_4$ as an example in the following, since $\text{Ba}_3\text{Zn}_2\text{As}_4$ and $\text{Ba}_3\text{Cd}_2\text{Sb}_4$ have similar results to that of $\text{Ba}_3\text{Cd}_2\text{As}_4$ and are presented in the Supplemental Material [31]. In the case without spin-orbit coupling (SOC) included, the calculated band structures within the generalized gradient approximation (GGA) show that two bands with opposite parity are inverted around the V and M points, as shown in Fig. 2(a). The inverted band structures lead to nodal lines near the Fermi level, which are protected by the time-reversal symmetry T and the inversion symmetry P [36–38]. Due to the constraint of the mirror symmetry $M_{1\bar{1}0}$, the crossing points form two 1D lines extending through the whole momentum space in the mirror plane. When SOC is taken into account, all nodes along the nodal lines open band gaps, as shown by the red dashed lines in Fig. 2(a). Due to the band gaps induced by SOC, the topological invariants Z_2 are well defined by a “curved chemical potential” which can be used to separate the valence and conduction bands. Its band topological invariants $Z_2 = (0; 110)$ can be easily calculated by the parity criterion proposed by Fu and Kane [39], which indicates these materials are weak TIs. Besides, there are two surface Dirac cones on both (001) and (010) surfaces (see the Supplemental Material [31] for more details).

C_2 anomalous surface states. The SIs $Z_{2,2,2,4} = (1102)$ for $\text{Ba}_3\text{Cd}_2\text{As}_4$ [22,23] have been obtained and two sets of topological invariants correspond to these SIs. Further calculations of the mirror Chern number ($\nu_{m_{1\bar{1}0}} = 0$) can distinguish them. We find the nontrivial topological invariant $\nu_{C_2} = 1$. The nonzero ν_{C_2} indicates that this material is a TCI with a C_2 rotation anomaly, which hosts two surface Dirac cones located on both the top and bottom $(1\bar{1}0)$ surfaces. If the sample is fabricated in a cylinder or prism along rotation axis $[1\bar{1}0]$, there will be two 1D helical hinge states related by C_2 rotation on the side surface as shown in Fig. 1(a).

To well identify the Dirac cones on the $(1\bar{1}0)$ surface, we calculate the surface states with a modified on-site energy of atoms in the outmost unit cell by increasing 0.06 eV. This is reasonable and widely used to simulate the different chemical environment of atoms in and beneath the surface. The results

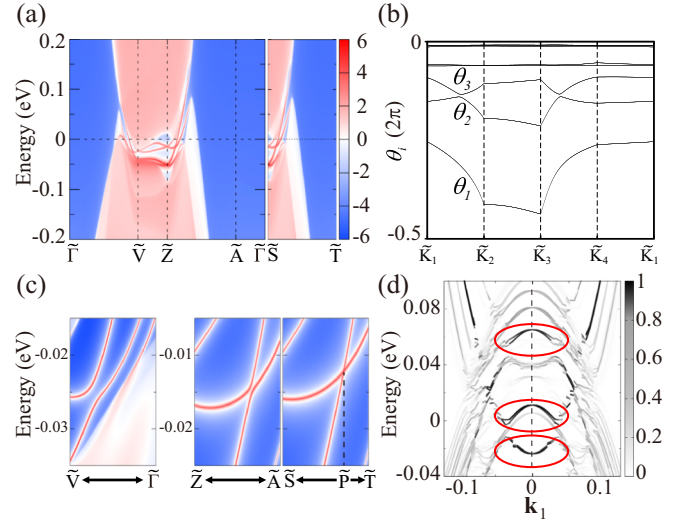


FIG. 3. (a) The $(1\bar{1}0)$ surface states of $\text{Ba}_3\text{Cd}_2\text{As}_4$ obtained from the GGA + SOC calculations. (b) The Wilson loop flow along a chosen loop $\tilde{K}_1\text{-}\tilde{K}_2\text{-}\tilde{K}_3\text{-}\tilde{K}_4\text{-}\tilde{K}_1$ which encloses a crossing point of two Wilson loop flows θ_2 and θ_3 . (c) The enlarged plot of $(1\bar{1}0)$ surface states along the $\tilde{V}\text{-}\tilde{\Gamma}$, $\tilde{Z}\text{-}\tilde{A}$, and $\tilde{S}\text{-}\tilde{T}$ paths. The surface Dirac cone is at \tilde{P} along $\tilde{S}\text{-}\tilde{T}$. (d) The helical hinge states are found along the \mathbf{k}_1 direction. The darker the color, the more weight of the wave function on the two hinges where the hinge states exist. The darkest bands marked with red circles are hinge states.

are shown in Fig. 3(a). The surface states open gaps along both $\tilde{\Gamma}\text{-}\tilde{V}$ and $\tilde{Z}\text{-}\tilde{A}$, as shown in the enlarged plots in Fig. 3(c). The Dirac cones at \tilde{V} and \tilde{Z} are trivial surface states since both of them can be pushed into valence or conduction bands without closing the band gap. However, there are two surface Dirac cones at generic momenta due to the C_2 anomaly on the $\tilde{S}\text{-}\tilde{T}$ path, which is off the high symmetrical line $\tilde{Z}\text{-}\tilde{A}$, as shown in Fig. 3(c). One surface Dirac cone locates at \tilde{P} ($-0.4673, 0.4375$) on the $(1\bar{1}0)$ surface BZ and the other one is related by C_2 rotation.

To demonstrate the existence of surface Dirac cones on the $(1\bar{1}0)$ surface, we calculate the Berry phase of the Wilson loop eigenfunctions based on the tight-binding Hamiltonian from the construction of maximally localized Wannier functions. Three new reciprocal lattice vectors \mathbf{k}_1 , \mathbf{k}_2 , and \mathbf{k}_3 as shown in Fig. 1(d) have been defined, where \mathbf{k}_1 is along the C_2 rotation axis while \mathbf{k}_2 and \mathbf{k}_3 form the surface BZ. The loop integral of the overlap matrix in Eq. (3) is along the reciprocal lattice \mathbf{k}_1 and the obtained Berry-Zak phase evolves along the loop $k_\lambda(k_2, k_3)$ in the $(1\bar{1}0)$ surface BZ. The Wannier centers $\theta_i(k_\lambda)$ and the eigenfunctions $\tilde{w}_i(k_\lambda)$ are calculated with all occupied bands of $n_{\text{occ}} = 22$ included in the effective Hamiltonian. It is well known that the Wilson loop flows have the same topological properties as the surface states. The Wilson loop flows along the high symmetrical paths in the surface BZ are shown in the Supplemental Material [31]. To identify the crossing point, we chose a k_λ loop composed of $\tilde{K}_1, \tilde{K}_2, \tilde{K}_3, \tilde{K}_4$, which in fact surrounds a crossing point of two Wilson loop flows θ_2 and θ_3 as shown in Fig. 3(b). There is gap between θ_2 and θ_3 along the loop. To show there is a crossing point between θ_2 and θ_3 inside of the loop, two eigenfunctions $\tilde{w}_{i=1,2}(k_\lambda)$ are taken as occupied states to calculate the Berry

phase along the loop according to Eq. (5). Thus, we obtain the π Berry phase, which proves the existence of the Dirac point.

Helical hinge states. As mentioned above, the helical 1D states can exist on the hinge where two gapped surfaces intersect each other, so that we take a prism geometry in Fig. S5(a) in the Supplemental Material [31] with open boundary conditions around all four side surfaces and a periodic boundary condition along the prism direction, namely, the C_2 rotation axis $[1\bar{1}0]$. We construct a tight-binding model of the new unit cell and calculate the band structure of a 6×6 supercell in Fig. 3(d). Because there is no direct band gap in the bulk states, the band structure of the supercell has no clear gap. To identify the hinge states, we calculate the weight of wave functions on the two hinges where the hinge states exist. The darkest bands are hinge states. The hinge states appear as a Dirac cone protected by C_2 and time-reversal symmetry at TRIM. They are localized at the two hinges (see the Supplemental Material [31]). The 4×4 and 10×10 supercells are also calculated (see the Supplemental Material [31]). We find the number of hinge states does not change for different sizes since the number of hinges is fixed, while the number of surface states and bulk states changes because of the changes of surface area and bulk volume for different sizes. The hinge states in the other prism geometry are also calculated, and the results are similar as shown in the Supplemental Material [31]. The hinge states are buried within the bulk and surface states. However, since hinge states have a dominant local density of states along the hinges, they might be measured by scanning tunneling microscopy (STM) similar to the hinge state measurement of bismuth [40].

Phase diagrams and topological phase transitions. Considering the well-known underestimation of the band gap within GGA, additional hybrid functional calculations in the Heyd-Scuseria-Ernzerhof (HSE06) scheme are performed to check the band inversion in $\text{Ba}_3\text{Cd}_2\text{As}_4$. As shown in Fig. 2(b), the band inversion within HSE06 only happens at M instead of both V and M within GGA. In view of the small band inversion depth, the band inversion might be adjusted by external strain. When the lattice constants are compressed by 6%, the band inversion appears at both V and M . However, when the lattice constants are expanded by 4%, there is no band inversion at either V or M . We also get similar results for $\text{Ba}_3\text{Zn}_2\text{As}_4$ and $\text{Ba}_3\text{Cd}_2\text{Sb}_4$ in the Supplemental Material [31].

Therefore, we can tune these materials into various topologically distinct states by the compression or expansion of lattice constants in the way of hydrostatic pressure. The phase diagrams about the bands at V and M , and the nodal lines in $\text{Ba}_3\text{Cd}_2\text{As}_4$ are shown in Fig. 4(a) under different strain. In the case without SOC, the band inversion only happens at M under zero pressure with lattice constants being a_0 , b_0 , and c_0 . When the lattice constants are compressed, the band inversion increases at M and the band gap closes at V , and band inversion appears at V as shown in Fig. 4(b). The critical point of the phase transition is at $a = b = 0.9643a_0$, $c = 0.9643c_0$. When the lattice constants are expanded, the band gap increases at V , while the band inversion disappears at M , as shown in Fig. 4(c). The critical point is at $a = b = 1.0305a_0$, $c = 1.0305c_0$. When SOC is considered, the $\text{Ba}_3\text{Cd}_2\text{As}_4$ is

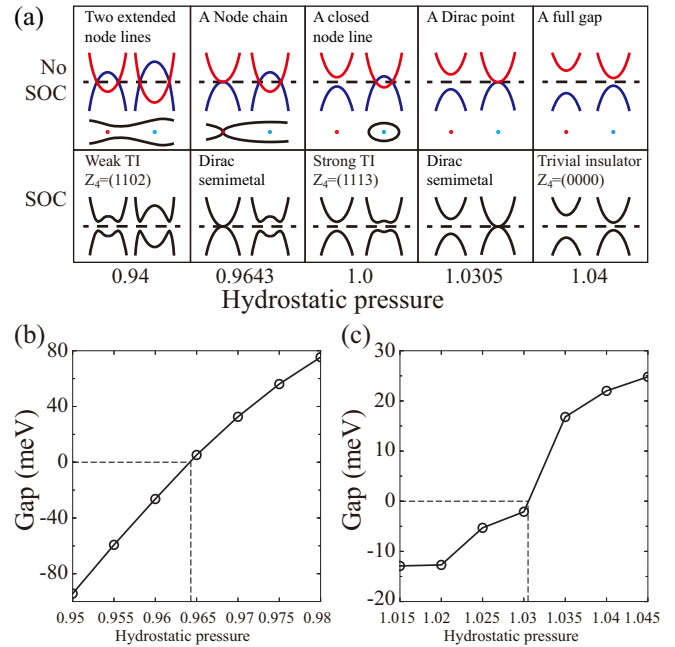


FIG. 4. (a) The topological phase transitions of $\text{Ba}_3\text{Cd}_2\text{As}_4$ under different hydrostatic pressures. The pressure is simulated by changing three lattice constants in the ratio of a_0 and c_0 within HSE06 calculations. The upper row shows bands (red and blue curves) close to the Fermi energy (black dashed lines) without SOC at V (red point) and M (cyan point). The black curves indicate the nodal lines around them. The lower row shows bands (black curves) with SOC included. (b) and (c) are the band gap change without SOC at the V point under compression and at M under expansion, respectively. The dashed lines indicate the phase transition critical points where the band gap closes.

a strong TI with $\mathbb{Z}_{2,2,2,4} = (1113)$ without pressure. It transforms from a strong TI to a TCI with $\mathbb{Z}_{2,2,2,4} = (1102)$, and to a normal insulator, respectively, and it becomes a Dirac semimetal at two critical points of the phase transition. Similar results can also be obtained for $\text{Ba}_3\text{Zn}_2\text{As}_4$ and $\text{Ba}_3\text{Cd}_2\text{Sb}_4$.

Conclusion. We demonstrate a new class of TCI with a C_2 rotation anomaly in Zintl compounds ($\text{Ba}_3\text{Cd}_2\text{As}_4$, $\text{Ba}_3\text{Zn}_2\text{As}_4$, and $\text{Ba}_3\text{Cd}_2\text{Sb}_4$) by first-principles calculations and SI analysis. When SOC is ignored, these materials are nodal line semimetals with two extended nodal lines in the mirror plane within the GGA calculation. With consideration of SOC, they become TCIs. There are only two surface Dirac cones protected by C_2 and time-reversal symmetry T at arbitrary momenta on both the top and bottom ($1\bar{1}0$) surfaces. The precise positions of the surface Dirac cones are determined by calculations of the ($1\bar{1}0$) surface states. We develop a nested Wilson loop method to prove the existence of surface Dirac cones. The helical hinge states on the side surface are also calculated. Within HSE06 calculations, we get the topological phase diagrams of $\text{Ba}_3\text{Cd}_2\text{As}_4$ under compression and expansion hydrostatic pressure. This new class of TCIs are experimentally synthesized and are to be verified by experiments. It provides us an ideal platform to study the C_2 rotation anomaly and high-order TIs with hinge states.

Acknowledgments. We acknowledge support from the Ministry of Science and Technology of China (Grants No. 2016YFA0300600, No. 2016YFA0302400, and No. 2018YFA0305700), the National Natural Science Foundation (Grants No. 11674370, No. 11421092, and No. 11674369), the Chinese Academy of Sciences (Grants No. XDB28000000

and No. XXH13506-202), the Science Challenge Project (TZ2016004), the K. C. Wong Education Foundation (GJTD-2018-01), the Beijing Natural Science Foundation (Z180008), and the Beijing Municipal Science and Technology Commission (Z181100004218001).

-
- [1] C. Fang and L. Fu, [arXiv:1709.01929](https://arxiv.org/abs/1709.01929).
- [2] R. Jackiw, *Phys. Rev. D* **29**, 2375 (1984).
- [3] G. W. Semenoff, *Phys. Rev. Lett.* **53**, 2449 (1984).
- [4] E. Fradkin, E. Dagotto, and D. Boyanovsky, *Phys. Rev. Lett.* **57**, 2967 (1986).
- [5] F. D. M. Haldane, *Phys. Rev. Lett.* **61**, 2015 (1988).
- [6] L. Fu, C. L. Kane, and E. J. Mele, *Phys. Rev. Lett.* **98**, 106803 (2007).
- [7] Y. Ando and L. Fu, *Annu. Rev. Condens. Matter Phys.* **6**, 361 (2015).
- [8] C.-K. Chiu, J. C. Y. Teo, A. P. Schnyder, and S. Ryu, *Rev. Mod. Phys.* **88**, 035005 (2016).
- [9] K. Shiozaki, M. Sato, and K. Gomi, *Phys. Rev. B* **95**, 235425 (2017).
- [10] M. Guo, K. Ohmori, P. Putrov, Z. Wan, and J. Wang, [arXiv:1812.11959](https://arxiv.org/abs/1812.11959).
- [11] Z. Song, Z. Fang, and C. Fang, *Phys. Rev. Lett.* **119**, 246402 (2017).
- [12] W. A. Benalcazar, B. A. Bernevig, and T. L. Hughes, *Science* **357**, 61 (2017).
- [13] F. Schindler, A. M. Cook, M. G. Vergniory, Z. Wang, S. S. P. Parkin, B. A. Bernevig, and T. Neupert, *Sci. Adv.* **4**, eaat0346 (2018).
- [14] J. Langbehn, Y. Peng, L. Trifunovic, F. von Oppen, and P. W. Brouwer, *Phys. Rev. Lett.* **119**, 246401 (2017).
- [15] W. A. Benalcazar, B. A. Bernevig, and T. L. Hughes, *Phys. Rev. B* **96**, 245115 (2017).
- [16] J. Liu, W. Duan, and L. Fu, *Phys. Rev. B* **88**, 241303(R) (2013).
- [17] T. H. Hsieh, H. Lin, J. Liu, W. Duan, A. Bansil, and L. Fu, *Nat. Commun.* **3**, 982 (2012).
- [18] T. H. Hsieh, J. Liu, and L. Fu, *Phys. Rev. B* **90**, 081112(R) (2014).
- [19] X. Zhou, C.-H. Hsu, T.-R. Chang, H.-J. Tien, Q. Ma, P. Jarillo-Herrero, N. Gedik, A. Bansil, V. M. Pereira, S.-Y. Xu, H. Lin, and L. Fu, *Phys. Rev. B* **98**, 241104(R) (2018).
- [20] F. Tang, H. C. Po, A. Vishwanath, and X. Wan, *Nat. Phys.* **15**, 470 (2019).
- [21] C.-H. Hsu, X. Zhou, Q. Ma, N. Gedik, A. Bansil, V. M. Pereira, H. Lin, L. Fu, S.-Y. Xu, and T.-R. Chang, *2D Mater.* **6**, 031004 (2019).
- [22] Z. Song, T. Zhang, Z. Fang, and C. Fang, *Nat. Commun.* **9**, 3530 (2018).
- [23] T. Zhang, Y. Jiang, Z. Song, H. Huang, Y. He, Z. Fang, H. Weng, and C. Fang, *Nature (London)* **566**, 475 (2019).
- [24] F. Tang, H. C. Po, A. Vishwanath, and X. Wan, *Nature (London)* **566**, 486 (2019).
- [25] M. G. Vergniory, L. Elcoro, C. Felser, N. Regnault, B. A. Bernevig, and Z. Wang, *Nature (London)* **566**, 480 (2019).
- [26] J. Wang, S.-Q. Xia, and X.-T. Tao, *J. Solid State Chem.* **198**, 6 (2013).
- [27] B. Saparov, S.-q. Xia, and S. Bobev, *Inorg. Chem.* **47**, 11237 (2008).
- [28] J. Jiang and S. M. Kauzlarich, *Chem. Mater.* **18**, 435 (2006).
- [29] A. P. Holm, S. M. Kauzlarich, S. A. Morton, G. D. Waddill, W. E. Pickett, and J. G. Tobin, *J. Am. Chem. Soc.* **124**, 9894 (2002).
- [30] I. R. Fisher, S. L. Bud'ko, C. Song, P. C. Canfield, T. C. Ozawa, and S. M. Kauzlarich, *Phys. Rev. Lett.* **85**, 1120 (2000).
- [31] See Supplemental Material at <http://link.aps.org/supplemental/10.1103/PhysRevResearch.1.012001> for (i) the crystallographic data of Zintl compounds, (ii) band structures and surface states of $Ba_3Zn_2As_4$ and $Ba_3Cd_2Sb_4$, and (iii) Wilson loop flow, surface states, and hinge states of $Ba_3Cd_2As_4$.
- [32] A. Alexandradinata, X. Dai, and B. A. Bernevig, *Phys. Rev. B* **89**, 155114 (2014).
- [33] R. D. King-Smith and D. Vanderbilt, *Phys. Rev. B* **47**, 1651 (1993).
- [34] V. Berry Michael, *Proc. R. Soc. London, Ser. A* **392**, 45 (1984).
- [35] D. Vanderbilt, *Berry Phases in Electronic Structure Theory: Electric Polarization, Orbital Magnetization and Topological Insulators* (Cambridge University Press, Cambridge, UK, 2018).
- [36] A. A. Burkov, M. D. Hook, and L. Balents, *Phys. Rev. B* **84**, 235126 (2011).
- [37] H. Weng, Y. Liang, Q. Xu, R. Yu, Z. Fang, X. Dai, and Y. Kawazoe, *Phys. Rev. B* **92**, 045108 (2015).
- [38] Q. Xu, R. Yu, Z. Fang, X. Dai, and H. Weng, *Phys. Rev. B* **95**, 045136 (2017).
- [39] L. Fu and C. L. Kane, *Phys. Rev. B* **76**, 045302 (2007).
- [40] F. Schindler, Z. Wang, M. G. Vergniory, A. M. Cook, A. Murani, S. Sengupta, A. Y. Kasumov, R. Deblock, S. Jeon, I. Drozdov *et al.*, *Nat. Phys.* **14**, 918 (2018).